Hindawi
Advances in Materials Science and Engineering
Volume 2022, Article ID 8622510, 16 pages
https://doi.org/10.1155/2022/8622510

Research Article

Unsteady Radiative Maxwell Fluid Flow over an Expanding Sheet with Sodium Alginate Water-Based Copper-Graphene Oxide Hybrid Nanomaterial: An Application to Solar Aircraft

S. Chandrasekaran,[1] **M. Satyanarayana Gupta**,[2] **Sanju Jangid**,[3] **K. Loganathan**,[3,4] **B. Deepa**,[5] **and Dinesh Kumar Chaudhary**[6]

[1]*Department of Mathematics, Government Arts and Science College, Idappadi 637102, Tamil Nadu, India*
[2]*Department of Aeronautical Engineering, MLR Institute of Technology, Hyderabad, Telangana, India*
[3]*Department of Mathematics and Statistics, Manipal University Jaipur, Jaipur 303007, India*
[4]*Research and Development Wing, Live4Research, Tiruppur 638106, Tamil Nadu, India*
[5]*Department of Mathematics, Faculty of Engineering, Karpagam Academy of Higher Education, Coimbatore, Tamil Nadu, India*
[6]*Department of Physics, Amrit Campus, Tribhuvan University, Kathmandu, Nepal*

Correspondence should be addressed to M. Satyanarayana Gupta; msngupta.m@gmail.com and Dinesh Kumar Chaudhary; din.2033@gmail.com

Received 18 July 2022; Revised 6 August 2022; Accepted 10 August 2022; Published 5 September 2022

Academic Editor: Pudhupalayam Muthukutti Gopal

The primary heat source from the sunlight is solar energy, which is used in photovoltaic panels, solar power plates, photovoltaic streetlights, and solar-based hybrid nanocomposites. A hybrid nanofluid is traversing an expanding sheet in this investigation. Maxwell fluid stream with two nanoparticles is going towards a trough with a parabolic form and is situated within the solar aircraft wing to investigate the phenomena of heat transfer rate. The term solar thermal radiation was introduced to describe heat transfer occurrence. The effectiveness of heat transmission from airplane wings is assessed by taking into account unique phenomena such as magnetic field and heat source. The bvp4c procedure was applied to quantitatively explain the energy and motion equations with MATLAB software. The copper (Cu) and graphene oxide (GO) nanosolid particles are mixed with sodium alginate (SA), a common liquid, to form the nanosolid particles. Numerous control variables are thoroughly examined, including temperature, shear stress, motion, friction component, and Nusselt number. The skin-friction coefficient upsurges with a growing magnetic impression. The upsurge in Deborah number reduces the skin-friction coefficient. The heat source impression declines the heat transport rate but upsurges the skin-friction coefficient. The skin-friction coefficient and heat transport rate increase with growing magnetic impression. When it comes to heat transfer analysis, hybrid nanofluid efficiency is substantially superior to that of regular nanofluid.

1. Introduction

The primary cause of pollution and increase in atmospheric CO2 concentrations is the production and consumption of energy; hence, lowering CO2 emissions and transitioning to carbon-free energy sources are essential for the sustainability of life on Earth. Experts are actively investigating the use of nanotech and solar radiation to improve the efficiency of flying. Analysts are now investigating how to use nanotech and sunshine radiation to increase the productivity of aircraft. Brewster [1] analysed and reported the nature of radiative heat transfer. By embedding microparticles in standard heat exchangers, Choi and Eastman [2] suggested that a whole new class of heat exchangers may be developed. Suresh et al. [3] studied heat transfer effects on laminar convective flow in a pressure droplet features past an unvaryingly rounded tube via Al_2O_3–Cu/water hybrid nanofluid. The power management plan for solar-powered

high-level long-endurance aircraft was researched by Gao et al. [4]. The size of a solar/hydrogen structure for high altitudes and long-endurance airplanes was covered by Barbosa et al. [5]. The flow and energy transport in top-convective Maxwell fluid above an exponentially stretched surface with the Cattaneo–Christov heat flux were subjected by Ahmad et al. [6]. As described in Das et al.'s [7] study, the computational analysis of the time-dependent laminar hydromagnetic boundary layer flow and energy transport of nanofluids across an accelerated convective heat heated stretched sheet. Current research on the production, thermal physical features, heat transmission, pressure drop features, potential uses, and limitations of hybrid nanofluids was compiled by Sarkar et al. [8]. An experiment on temperature and nanosized particles volume with thermal conductivity of $ZnO–TiO_2$/EG hybrid nanofluid was investigated by Toghraie et al. [9].

Efficacy in energy transport is currently the most important requirement from an industry standpoint. Modern businesses will not be able to function with conventional cooling solutions. Nanofluids have great promise as effective heat transfer devices. Microchooses, 100 nm metering, are involved in this phenomenon and can be detected in ethylene, water, oil, or glycol. Typically, the metals, oxide, carbon graphite, nitrides, carbides, and nanotubes are confined in nanostructures. Since then, numeral techniques have been established in a direction to increase the heat exposure of nanofluids. Nanoparticles, heat diffusion, Brownian motion, thermophoresis, and other techniques are among them. Using the Buongiorno model, Farooq et al. [10] examined hydromagnetic Maxwell fluid with nanomaterials on a surface that is extending exponentially while also accounting for thermophoretic and Brownian motion phenomena. Loganathan et al. [11] cast off the Cattaneo–Christov heat flux model to study the impact of second-order slip, reaction rate, and cross-diffusion properties on the hydromagnetic convective Oldroyd-B liquid flow towards a stretchable surface. Maleki et al. [12] inspected the impression of the Eckert amount, temperature and motion slipping parameters, radiation, suction or blowing, heat source/sink, and tiny particle volume fraction on the motion and heat transmission on the flow and heat transmission over a porous plain plate.

The research about non-Newtonian fluids has recently attracted a lot of interest. This is due to their wide range of industrial product applications. A most crucial factor in geoscience, biomechanics, and industries is how fluids flow through the porous material, including water through rock, to regulate skin temperature and filter out impurities. Typically, more than one fundamental equation cannot adequately describe these fluids. Due to the variety of these fluids, many constitutive equations are therefore presented. The three primary categories of non-Newtonian fluids are integral, rate, and differential kinds. The nonviscous fluids rate type includes Maxwell fluid. This lesson highlights the benefits of downtime. Abdelmalek et al. [13] analyzed the double-diffusion occurrence in Carreau liquid transient, a wedge-formed frame with strain relations and connections for heat physical features. The advancements in the primary cycles and relevant features, CSP (Concentrated Solar Power) techniques, heat exchange, and phase transition substance applied for thermal energy storage were the main topics of Khandelwal et al.'s [14] study of the integrated solar combined cycle system. The thermally stratiform flow of Oldroyd-B liquid caused by a stretchable sheet was explored by Loganathan et al. [15] with the effects of radiation and chemical reactions. To perform better, Rubbi et al. [16] developed a working fluid from soybean oil and Ti_3C_2 particles for use in a hybrid photovoltaic-thermal (PV-T) solar gatherer. Loganathan et al. [17] discovered the entropy investigation of third-order nanofluid flow with the impression of inclined magnetic impact across a convective surface. Loganathan et al. [18] addressed the impression of hydromagnetic Darcy–Forchheimer third-grade nanofluid flow towards a linear elastic sheet. Waini et al. [19] evaluated the constant mixed convective for both assisting and opposing flows over an erect surface immersed in a porous mode with Al_2O_3–Cu/water hybrid nanofluid. Through the development of a total energy optimizing model that incorporates the connection of increased energy conversion and additional energy usage, Wu et al. [20] concentrated on evaluating the energy concert of a symmetrical Λ-formed movable arm solar aircraft.

Usage for the impacts of magnetic influence on non-Newtonian fluids is expanding in a variety of industries, including chemical engineering, polymeric technologies, MHD generators, nuclear reactors, petroleum industries, and acceleration, geothermal heat, and plasma investigations. Ahmad et al. [21] studied an applied magnetic field, thermal dissipation, a heat source, and convective boundary circumstances; heat transfer is theoretically enhanced for graphene oxide/kerosene oil and graphene oxide-silver/kerosene oil hybrid nanofluids over a porous stretchable sheet. By employing hybrid nanofluid (CNT (carbon nanotube)-Al_2O_3/water and CNT-Fe3O4/water) as a cooling under the encouragement of an external magnetic field, Anitha et al. [22] inspected the energy transference performance of an advanced manufacturing double-tube heat exchanger. Gul et al. [23] discovered the heat insulation of the hybrid nanofluid flow in four distinct scenarios of conical gap between a cone and disc flow, involving 1st static cone revolving disc, 2nd static cone spinning disc, 3rd cone and disk rotation in much the same way, and 4th cone and disc rotation in the opposite direction. In the company of the convective situation, Hussain et al. [24] concentrated on hybrid nanoliquid flow through an exponentially extending spinning surface. The thermal characteristics of the moving copper-iron (II, III)/oxide-engine oil Casson fluid with nanoparticles in the solar parabolic trough absorber were explored by Jamshed et al. in [25]. To deepen the experiments of the sunlight aircraft wings with different assets like porous mode, Cattaneo–Christov heat flux, viscosity dissipation, heating and flow of energy, and entropy creation, Jamshed et al. [26] researched heat exchange by utilizing the tangent hyperbolic nanocomposite past inside solar wings

solar parabolic trough receiver. Jamshed et al. [27] evaluated the flow and heat transmission characteristics of a Cu–TiO_2/tangent hyperbolic hybrid nanofluid of this sort across a slippery surface. The temperature distribution and entropy creation analysis of third-grade nanofluid flow forward into stretchy sheet with oriented magnetic impacts, thermal radiation, heat source/sink, and convective thermal influences was researched by Jamshed [28]. Loganathan et al. [29] utilized a third-grade fluid flow with nanoparticles with zero mass flux and a non-Fourier model to analyze entropy and heat transfer. With the assistance of Cattaneo–Christov dual diffusion, Loganathan et al. [30] defined the effect of the hydrodynamic radiative Maxwell fluid model on a hot surface. Jamshed et al. [31] investigated radiative Prandtl–Eyring hybrid nanofluid in a parabolic trough surface within a solar water pump to analyze the viscid dissipation, heat generation, and entropy. Muhammad et al. [32] researched the time-dependent squeezing flow of a hybrid nanofluid (having CNTs + CuO/water) and a nanofluid (having CNTs/water) with the melting impact and viscid dissipation to designate the behavior of heat exchange, entropy formation, and bean amount. To optimize the creation of entropy of Williamson fluid flow towards a plain and stretchy surface, Qayyum et al. [33] tested the influence of hydromagnetic, nonlinear thermal radiation, Darcy–Forchheimer porous mode, viscous dissipation, 1st-order motion slip, and convective boundary circumstance. To manage the flow system heat transfer, Saeed et al. [34] employed the slip conditions created by a whirling disc, thermal stratification, and nonlinear thermal radiation in the solution of the Darcy–Forchheimer flow for TiO_2–Ag/H_2O hybrid nanofluid. The time-dependent Maxwell Cu–Al_2O_3/sodium alginate hybrid nanofluid approaching a stretchy/shrinking surface with radiative heat action and energy transmission was researched by Zainal et al. [35].

Several academics have been interested in the flow of a viscous caused by a stretched sheet. This is a result of their many uses in the polymeric industry worldwide, environmental contamination, biological processes, aerodynamic extraction of plastic sheets, manufacture of glass fiber along a liquid film and condensation process, chilling and/or dryness of papers and textile, and so on. Ahmad et al. [36] investigated the effects of brick-shaped nanostructured materials made of cerium oxide (CeO_2) and zinc oxide (ZnO) on the time-dependent three-dimensional water-driven hybrid nanofluid flow. In addition to the benefits of thermal defeat and the non-Fourier concept for energy flux, Algehyne et al. [37] revealed the heat transport in Maxwell MoS_2–Ag/engine oil hybrid nanofluid past across an endless stretchy erect porous sheet. Bhattacharyya et al. [38] inspected an electrically conducted Maxwell hybrid nanofluid fluid covering Cu and graphene oxide nanoparticles with time-dependent aligned magnetic field and velocity slip conditions over a linearly stretched sheet. On a convectively heated Riga plate with Cattaneo–Christov theory, Eswaramoorthi et al. [39] deliberated the effects of glycerin-based carbon nanotubes with motion slip in a porous material described by Darcy and Forchheimer. Ouni et al. [40] discussed the heat generation and viscous dissipation impression of Oldroyd-B fluid flow with copper-gold/engine oil hybrid nanoparticles with a parabolic trough surface collector within a solar water pump. Ali et al. [41] discussed the heat transportation and energy creation of carboxymethyl cellulose water-based cross hybrid nanofluid flow. Iftikhar et al. [36] researched the influence of heat generation/absorption of three-dimensional time-dependent brick from zinc-oxide hybrid nanofluid. A study on MHD radiative bidirectional hybrid nanofluid flow to analyze thermal performance was deliberated by Iftikhar et al. [42]. Iftikhar et al. [43] inspected the heat transference of blade-formatted cadmium telluride-graphite nanocomposites hybrid nanofluid flow under electromagnetohydrodynamics. Iftikhar et al. [44] studied an entropy creation of sphere-sized bidirectional hybrid nanofluid along with varying thermal performance. Using the Williamson model, Hussain [45] investigated the viscous dissipation, thermal radiation, and entropy creation of a hybrid nanofluid (Cu-graphene oxide/sodium alginate) that was situated within solar airplane wings and moved into a trough with a parabolic form. According to Jamshed et al. [46], time-independent hybrid nanofluid (Cu-silicon dioxide/engine oil) flow and thermal transport properties are affected by nanosolid particle morphologies, porosity substantial, heat generator, viscid dissipative, and radiative flux.

In solar aircraft wings, a trough with a parabolic shape called (PTSC) captures solar thermal energy in the system of solar radiative sprinkling. The quest for more expensive and alternative fuel sources will be significantly impacted by aviation studies. The heat transference rate increases when established hybrid nanofluids are used in place of conventional nanofluids. Because they were obtained under entirely cutting-edge substantial circumstances, the research findings will be helpful to fresh scientists.

The latest results can aid in future advancements by allowing for the assessment of the thermal system heat effect while taking into consideration various non-Newtonian hybrid nanofluids (Carreau, second-grade, tangent hyperbolic fluid, Casson, micropolar nanofluids, etc.). Furthermore, the extending approach may be used to simulate the effects of magneto-slip movement as well as temperature-dependent fluidity and porosity.

The research model may plug the space in heat transmission by utilizing radiative Maxwell hybrid nanofluid flows on a penetration stretchable surface, changing thermal conductivity, heat source, and MHD (magnetohydrodynamic) impact. The theoretical motion of the nanofluids is represented using the Tiwari and Das model. In this study, copper (Cu) and graphene oxide (GO) hybrid nanoparticles are used, with sodium alginate (SA) serving as the regular fluid. The Maxwell hybrid nanofluid's leading equation will be converted into ordinary differential equations with the proper parallel transformations.

2. Mathematical Formulation

The following are the circumstances and guiding principles that govern the flow model:

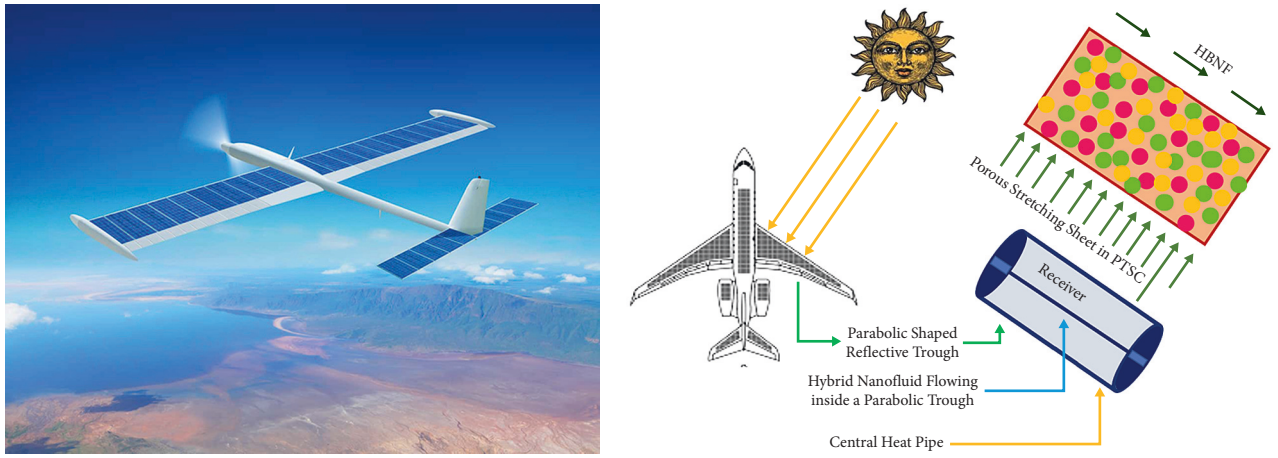

(a) (b)

Figure 1: Methodical picture of existing theoretic research.

(i) Two-dimensional unsteady laminar flow.
(ii) Boundary layer guesstimates.
(iii) Tiwari–Das model (single stage system).
(iv) Radiative Maxwell hybrid nanofluid.
(v) Piercing mode.
(vi) On the x-axis, a magnetic field $B(t) = B_0(1-\xi t)^{-(1/2)}$ is applied.
(vii) Flow with heat source and viscous dissipation.

The solar aircraft application modelling and flow diagram are given in Figures 1 and 2, respectively. Below mentioned equations are the governing equation [21, 45] for existing research work:

Equation of continuity:

$$\frac{\partial \mathrm{u}}{\partial \mathrm{x}} + \frac{\partial \mathrm{v}}{\partial \mathrm{y}} = 0. \tag{1}$$

Equation of motion:

$$\rho_{hbnf}\left(\frac{\partial \mathrm{u}}{\partial \mathrm{t}} + \mathrm{u}\frac{\partial \mathrm{u}}{\partial \mathrm{x}} + \mathrm{v}\frac{\partial \mathrm{u}}{\partial \mathrm{y}}\right) = \mu_{hbnf}\frac{\partial^2 \mathrm{u}}{\partial \mathrm{y}^2} - \lambda\left(\mathrm{u}^2\frac{\partial^2 \mathrm{u}}{\partial \mathrm{x}^2} + \mathrm{v}^2\frac{\partial^2 \mathrm{u}}{\partial \mathrm{y}^2} + 2uv\frac{\partial^2 \mathrm{u}}{\partial x \partial y}\right) - \sigma_{hbnf}B_0(t)^2 u - \mu_{hbnf}\frac{\mathrm{u}}{\mathrm{k}}. \tag{2}$$

Equation of temperature:

$$\left(\rho C_p\right)_{hbnf}\left(\frac{\partial T}{\partial t} + u\frac{\partial T}{\partial x} + v\frac{\partial T}{\partial y}\right) = k_{hbnf}\frac{\partial^2 T}{\partial y^2} - \frac{\partial q_r}{\partial y} + \mu_{hbnf}\left(\frac{\partial u}{\partial y}\right)^2 + Q_0(T - T_\infty). \tag{3}$$

The boundary situations for the present situation are as tracks [31, 40]:

$$u = U_w + N_w\frac{\partial u}{\partial y}, v = V_w, -k_0\left(\frac{\partial T}{\partial y}\right) = h_f(T_w - T), at\ y = 0, u \longrightarrow 0, T \longrightarrow T_\infty, at\ y \longrightarrow \infty. \tag{4}$$

The apparatuses of velocity in the consistent coordinates of y and x are meant by v (m/s) and u (m/s), respectively, where T (K) is the fluid temperature, λ is the relaxation time, N_w depicts the slip length, $\mathrm{V_w}$ signifies the encompassing plate porosity, and k_0 shows the material porousness. Furthermore, *hbnf* stands for hybrid nanofluid, *nf* stands for nanofluid, *Bf* stands for base fluid, $(\rho C_p)_{hbnf}$ denotes the heat capacity of the hybrid nanofluid, B_0 (Tesla-T) depicts the magnetic field strength, σ_{hbnf} depicts the electrical conductivity, k_{hbnf} denotes the thermal conductivity of the hybrid nanofluid, ρ_{hbnf} denotes the hybrid nanofluid density, and μ_{hbnf} denotes the hybrid nanofluid dynamic

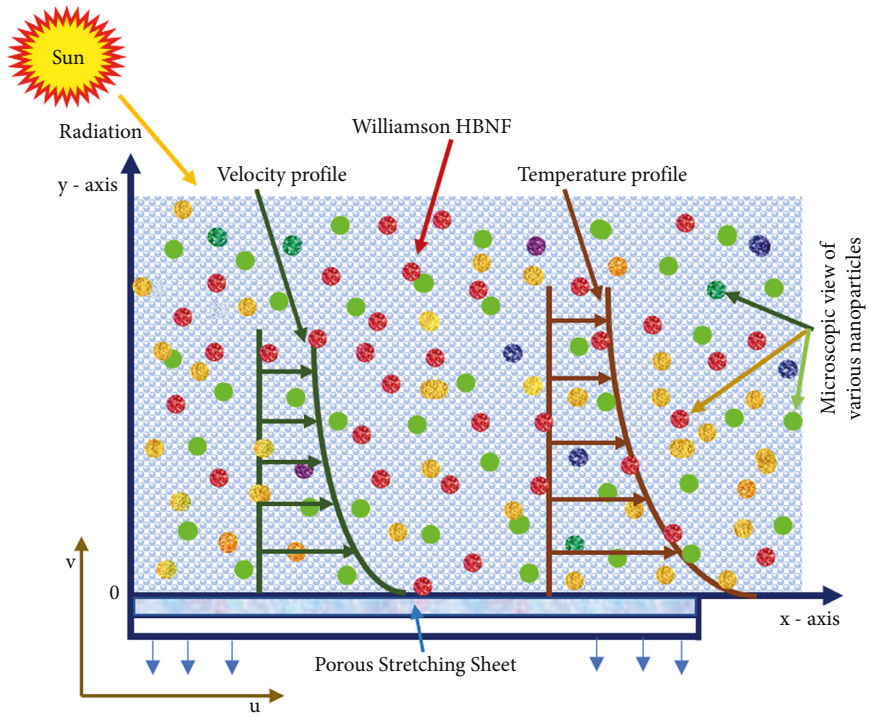

Figure 2: Movement model picture.

viscosity.C_p is the specific heat at unvarying pressure, M depicts the shape factor (3 for sphere), ϕ_{Cu} depicts the volume fraction of Cu, ϕ_{GO} depicts the volume fraction of GO, and $k_{Bf}, \mu_{Bf}, \rho_{Bf}$, and σ_{Bf} denote the thermal conductivity, dynamic viscosity, density, and electrical conductivity of the SA base fluid, respectively. The subscripts Bf, Cu, and GO denote the amounts of base fluid, Cu nanoparticle, and GO nanoparticle, respectively. As a result, Table 1 contains information on the working pure fluid as well as two different nanomaterials Cu and GO, and the hybrid nanoparticle physical properties are given in Table 2.

The penultimate term in energy (3), where q_r indicates the radiative heat flux and is delineated using the Rosseland guesstimate [38, 45], represents thermal radiation

$$q_r = \frac{-4\sigma^*}{3k^*}\frac{\partial T^4}{\partial y}, \tag{5}$$

where σ^* is the Stefan–Boltzmann constant and k^* corresponds to the coefficient of mean absorption. Now, using the Taylor series for the term T^4 at a location T_∞ and disregarding the higher order terms in approximation, the following final form may be obtained.

Here, T^4 is a linear connection of temperature through Taylor's arrangement extension about T_∞ and disregarding progressive terms; thus,

$$T^4 \approx 4T_\infty^3 T - 3T_\infty^4. \tag{6}$$

In the current situation, we may simplify our model analysis by taking into account the following nondimensional variables [19, 38, 45]:

$$\eta = \sqrt{\frac{b}{\nu_{Bf}(1-\xi t)}}y, \psi = \sqrt{\frac{\nu_{Bf} b}{(1-\xi t)}}x f, \theta(\eta) = \frac{T - T_\infty}{T_w - T_\infty}, u = \frac{\partial \psi}{\partial y} = \frac{bx f'}{(1-\xi t)} \text{ and } v = -\frac{\partial \psi}{\partial x} = -\sqrt{\frac{\nu_{Bf} b}{(1-\xi t)}} f. \tag{7}$$

The primes now stand for differentiation of the pseudosimilarity variables. According to the scientific flow model, a traveling flat plate with an uneven expansion motion and an isolating surface temperature is summarized as follows [38, 45]:

$$U_w = \frac{bx}{(1-\xi t)} \text{ and } T_w = T_\infty + \frac{b^* x}{(1-\xi t)}, \tag{8}$$

where the initial expansion rate and heat variance, respectively, are denoted by b and b^*. The temperatures of the surface and surroundings are represented, respectively, by

Table 1: The formulation and limitations for the nanofluid and hybrid nanofluid in the aforesaid system of equations [21, 45].

Thermal properties	Nanofluid	Hybrid nanofluid
Thermal diffusivity	$\alpha_{nf} = k_{nf}/(\rho C_p)_{nf}$	$\alpha_{hbnf} = k_{hbnf}/(\rho \mathrm{C_p})_{hbnf}$
Viscosity	$\mu_{nf}/\mu_{Bf} = 1/(1-\phi_{Cu})^{2.5}$	$\mu_{hbnf}/\mu_{Bf} = 1/(1-\phi_{Cu})^{2.5}(1-\phi_{GO})^{2.5}$
Heat capacity	$(\rho C_p)_{nf}/(\rho C_p)_{Bf} = ((1-\phi_{Cu}) + \phi_{Cu}(\rho C_p)_{Cu}/(\rho C_p)_{Bf})$	$(\rho \mathrm{C_p})_{hbnf}/(\rho \mathrm{C_p})_{Bf} = \phi_{GO}(\rho \mathrm{C_p})_{GO}/(\rho \mathrm{C_p})_{Bf} + (1-\phi_{GO})((1-\phi_{Cu}) + \phi_{Cu}(\rho \mathrm{C_p})_{Cu}/(\rho \mathrm{C_p})_{Bf})$
Density	$(\rho)_{nf}/(\rho)_{Bf} = ((1-\phi_{Cu}) + \phi_{Cu}(\rho)_{Cu}/(\rho)_{Bf})$	$(\rho)_{hbnf}/(\rho)_{Bf} = \phi_{GO}(\rho)_{GO}/(\rho)_{Bf} + (1-\phi_{GO})((1-\phi_{Cu}) + \phi_{Cu}(\rho)_{Cu}/(\rho)_{Bf})$
Thermal conductivity	$k_{nf} = k_{Cu} + (M-1)k_{Bf} - (M-1)\phi_{Cu}(k_{Bf} - k_{Cu})$ $/k_{Cu} + (M-1)k_{Bf} + \phi_{Cu}(k_{Bf} - k_{Cu})k_{Bf}$	$k_{hbnf} = k_{GO} + (M-1)k_{nf} - (M-1)\phi_{GO}(k_{nf} - k_{GO})/k_{GO}$ $+(M-1)k_{nf} + \phi_{GO}(k_{nf} - k_{GO})k_{nf}$
Electrical conductivity	$\sigma_{hbnf} = (1 + 3(\phi_{Cu}\sigma_{Cu}/\sigma_{Bf} - (\phi_{Cu}))/(\phi_{Cu}\sigma_{Cu}/(\phi_{Cu})\sigma_{Bf} + 2)$ $-(\phi_{Cu}\sigma_{Cu}/\sigma_{Bf} - (\phi_{Cu})))$	where, $k_{nf} = k_{Cu} + (M-1)k_{Bf} - (M-1)\phi_{Cu}(k_{Bf} - k_{Cu})/k_{Cu} + (M-1)k_{Bf} + \phi_{Cu}(k_{Bf} - k_{Cu})k_{Bf}$ $\sigma_{hbnf} = (1 + 3(\phi_{Cu}\sigma_{Cu} + \phi_{GO}\sigma_{GO}/\sigma_{Bf} - (\phi_{Cu} + \phi_{GO}))$ $/(\phi_{Cu}\sigma_{Cu} + \phi_{GO}\sigma_{GO}/(\phi_{Cu} + \phi_{GO})\sigma_{Bf} + 2) - (\phi_{Cu}\sigma_{Cu} + \phi_{GO}\sigma_{GO}/\sigma_{Bf} - (\phi_{Cu} + \phi_{GO})))$

Table 2: *Cu – GO/SA* hybrid nanoparticle physical properties [38, 45].

Physical characteristics	SA	Cu	GO
ρ	989	8933	1800
C_p	4175	385.0	717
k	0.6376	401.00	5000
σ	2.6×10^{-4}	5.96×10^{7}	1.1×10^{-5}
Pr	6.5	-	-

Table 3: Evaluation concerning the values of $-\theta'(0)$ with Pr, when $Bi \longrightarrow \infty$, and absenteeism of further remaining parameters.

Pr	Das et al. [7]	Jamshed et al. [25]	Hussain [45]	Current work
1	1.00000000	1.00000000	1.00000000	1.00000000
3	1.92357431	1.92357420	1.92357420	1.923682566
7	3.07314679	3.07314651	3.07314651	3.072250191
10	3.72055436	3.72055429	3.72055429	3.720673886

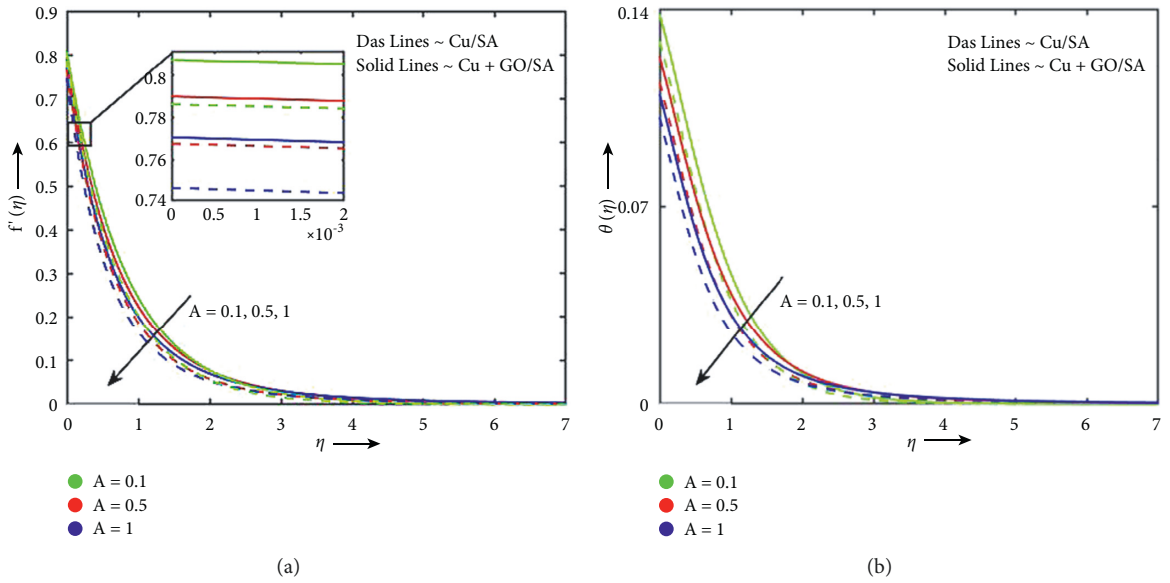

Figure 3: *A* variances in velocity and temperature.

T_w and T_∞. Temperature fluctuation puts the plate surface in harm because it is designed to be slick.

Using the similarity modifications (7), create controlling equations (1)–(4), where continuity (1) is completely fulfilled and the other required equations adopt the dimensionless form shown as follows:

$$f''' + \phi_a\phi_b f f'' - \phi_a\phi_b (f')^2 - \phi_a\phi_b \frac{\xi}{b} f' - \phi_a\phi_b \frac{\xi}{b}\frac{\eta}{2} f'' - Kf' - \beta\left(\phi_a\phi_b f^2 f''' - 2\phi_a\phi_b f f' f''\right) - \phi_a\phi_e Mn^2 f' = 0, \tag{9}$$

$$\theta''\left(1 + \frac{1}{\phi_d} PrNr\right) + \Pr\frac{\phi_c}{\phi_d}\left(f\theta' - f'\theta - A\left(\theta + \frac{\eta}{2}\theta'\right) + \frac{Ec}{\phi_a\phi_c} f''^2 + \frac{1}{\phi_c} Q\theta\right) = 0, \tag{10}$$

with the boundary circumstances

$$\begin{aligned} f(0) = S, f'(0) &= 1 + \Lambda f'', \theta'(0) \\ &= -Bi(1-\theta), at\ \eta = 0. f'(\infty) \\ &\longrightarrow 0, \theta(\infty) \longrightarrow 0, at\ \eta \longrightarrow \infty. \end{aligned} \tag{11}$$

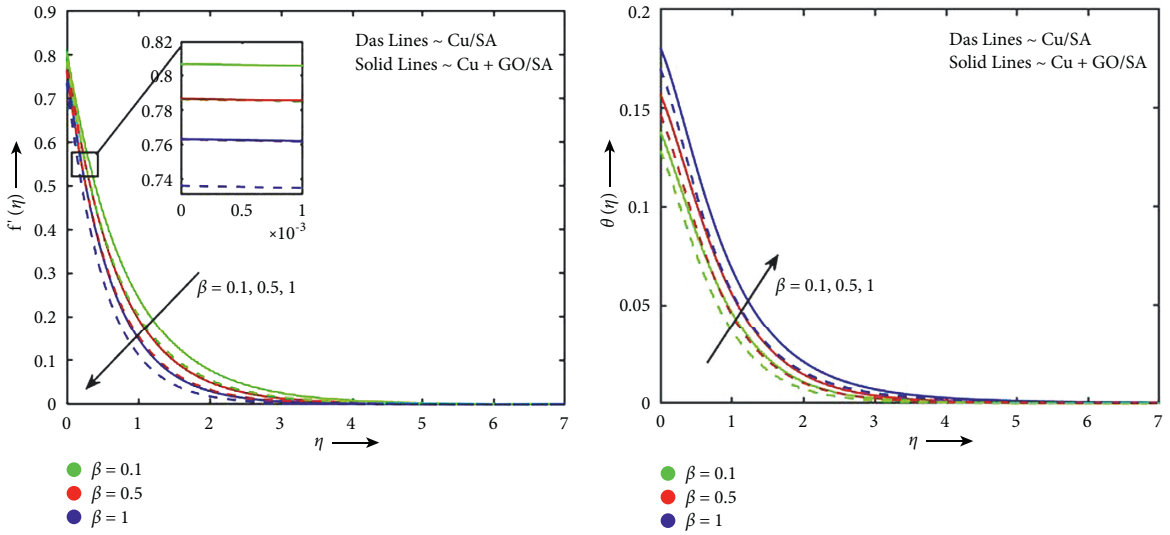

Figure 4: β variances in velocity and temperature.

The unsteadiness parameter (A), porous medium parameter (K), Deborah number (β), Hartmann (magnetic) parameter (Mn), Eckert number (Ec), heat source parameter (Q), Prandtl number (Pr), radiation parameter (Nr), suction/injection parameter (S), velocity slip parameter (Λ), and Biot number (Bi) are all terms used to describe the participation of dimensionless restrictions in equations (9)–(11). These variables are stated numerically as

$$\phi_a = \frac{\mu_{Bf}}{\mu_{hbnf}}, \phi_b = \frac{(\rho)_{hbnf}}{(\rho)_{Bf}}, \phi_e = \frac{(\sigma)_{hbnf}}{(\sigma)_{Bf}}, \phi_c = \frac{\left(\rho C_p\right)_{hbnf}}{\left(\rho C_p\right)_{Bf}},$$

$$\phi_d = \frac{(k)_{hbnf}}{(k)_{Bf}}, A = \frac{\xi}{b}, K = \frac{\nu_{Bf}(1-\xi t)}{bk}, \beta = \frac{\lambda U_w}{x},$$

$$Mn^2 = \frac{\sigma_{Bf} B_0^2}{\rho_{Bf} b}, Ec = \frac{U_w^2}{\left(C_p\right)_{Bf}(T_w - T_\infty)}, Q = \frac{Q_0 x}{\left(\rho C_p\right)_{Bf} U_w}, \quad (12)$$

$$\Pr = \frac{\nu_{Bf}}{\alpha_{Bf}}, Nr = \frac{16\sigma^* T_\infty^3}{3k^* \nu_{Bf}\left(\rho C_p\right)_{Bf}}, S = -V_w\sqrt{\frac{(1-\xi t)}{b\nu_{Bf}}},$$

$$\Lambda = \sqrt{\frac{b}{(1-\xi t)\nu_{Bf}}} N_w, Bi = \frac{h_f}{k_0}\sqrt{\frac{\nu_{Bf}(1-\xi t)}{b}}.$$

The shear stress and heat transport rate are the physical quantities of engineering practical significance, and they are delineated as follows.

The shear stress is $C_f = \tau_w/\rho_{Bf} U_w^2$, and the Nusselt number is well-defined as $\mathrm{Nu}_x = \mathrm{xq_w}/\mathrm{k}_{Bf}(T_w - T_\infty)$.

The surface shear stress τ_w is assumed by $\tau_w = \mu_{hbnf}(\partial u/\partial y)_{y=0}$, and we get

$$C_f Re_x^{1/2} = \frac{1}{\phi_a}[f''(0)]. \quad (13)$$

The rate of heat transfer q_w is assumed by $q_w = -k_{hbnf}(\partial \mathrm{T}/\partial y)_{y=0} + (q_r)_{y=0}$, and we get

$$Nu_x Re_x^{-1/2} = -\phi_d[1 + Nr]\theta'(0), \quad (14)$$

where $Re_x = xu_w/\nu_{Bf}$ is the Reynolds number.

3. Numerical Structure

Equations are solved via the bvp4c technique. All numerical values and graphs are found with MATLAB software which is discussed in through tables and graphs. Let

$$f = y(1), f' = y(2), f'' = y(3), \theta = y(4), \theta' = y(5). \quad (15)$$

Equations (9)–(11) are reduced into a new form as

$$f''' + \phi_a\phi_b y(1)y(3) - \phi_a\phi_b (y(2))^2 - \phi_a\phi_b\frac{\xi}{b} y(2) - \phi_a\phi_b\frac{\xi}{b}\frac{\eta}{2} y(3) - Ky(1)$$

$$-\beta\left(\phi_a\phi_b\left(y(1)\right)^2 f''' - 2\phi_a\phi_b y(1)y(2)y(3)\right) - \phi_a\phi_e Mn^2 y(2) = 0, \theta''\left(1 + \frac{1}{\phi_d} PrNr\right) \quad (16)$$

$$+ \Pr\frac{\phi_c}{\phi_d}\left(y(1)y(5) - y(2)y(4) - A\left(y(4) + \frac{\eta}{2} y(5)\right) + \frac{Ec}{\phi_a\phi_c}(y(3))^2 + \frac{1}{\phi_c} Qy(4)\right) = 0,$$

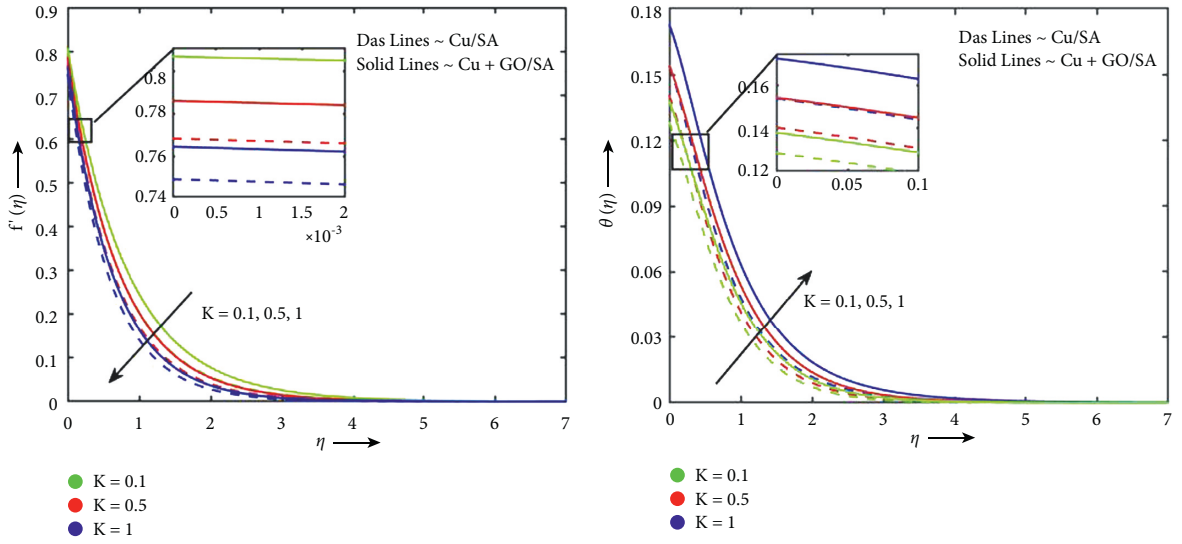

Figure 5: K variances in velocity and temperature.

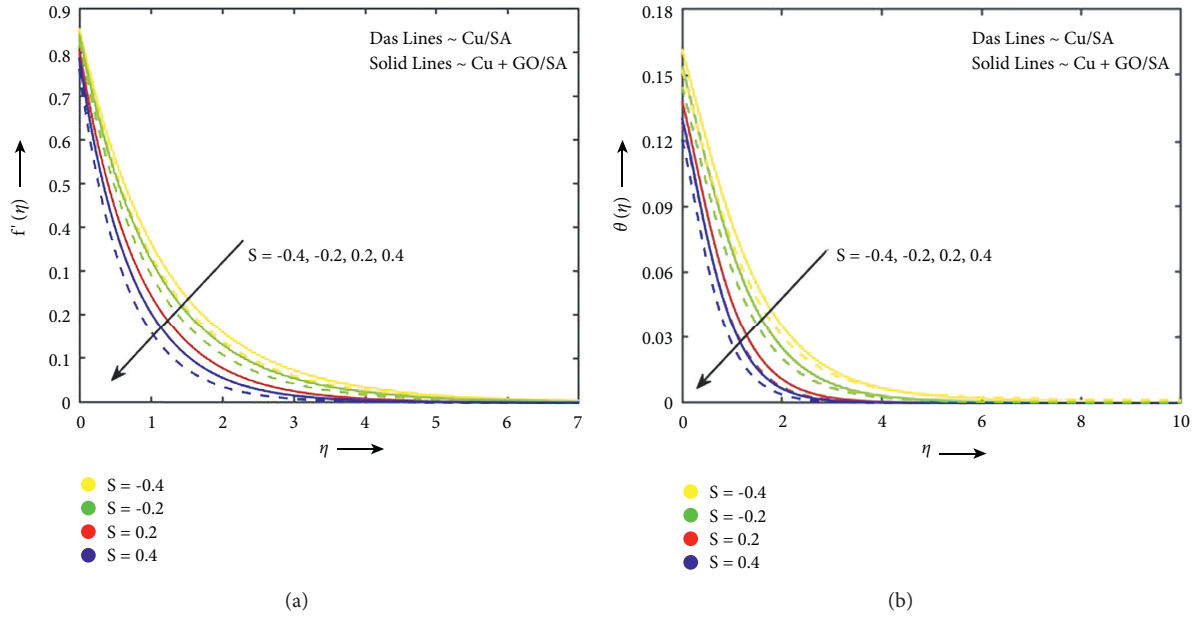

Figure 6: S variances in velocity and temperature.

with the boundary conditions

$$y0(1) = S, y0(2) = 1 + \Lambda y0(3), y0(5) = -Bi(1 - y0(4)), at\ \eta = 0 y\infty(2) \longrightarrow 0, y\infty(4) \longrightarrow 0, at\ \eta \longrightarrow \infty. \quad (17)$$

The choice $\eta(\infty) = 7$ or 10 indicates that each numerical output approaches asymptotic assets ideally in this technique.

3.1. Code Validation. Validation of present findings is carried out with the use of contrast to current research. Table 3 provides a comparison of the known research

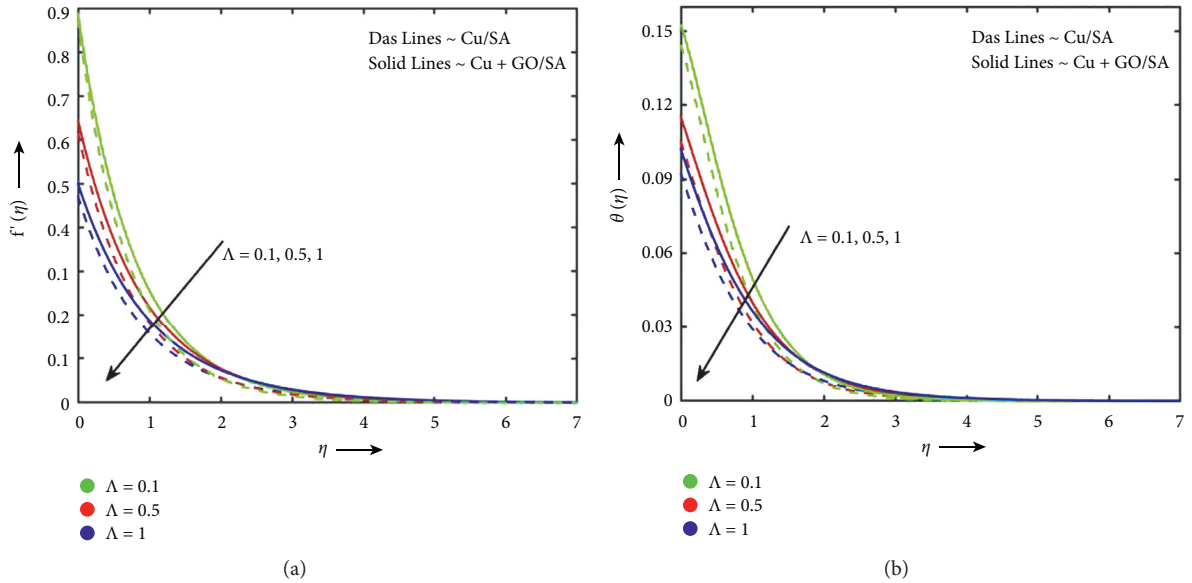

Figure 7: Λ variances in velocity and temperature.

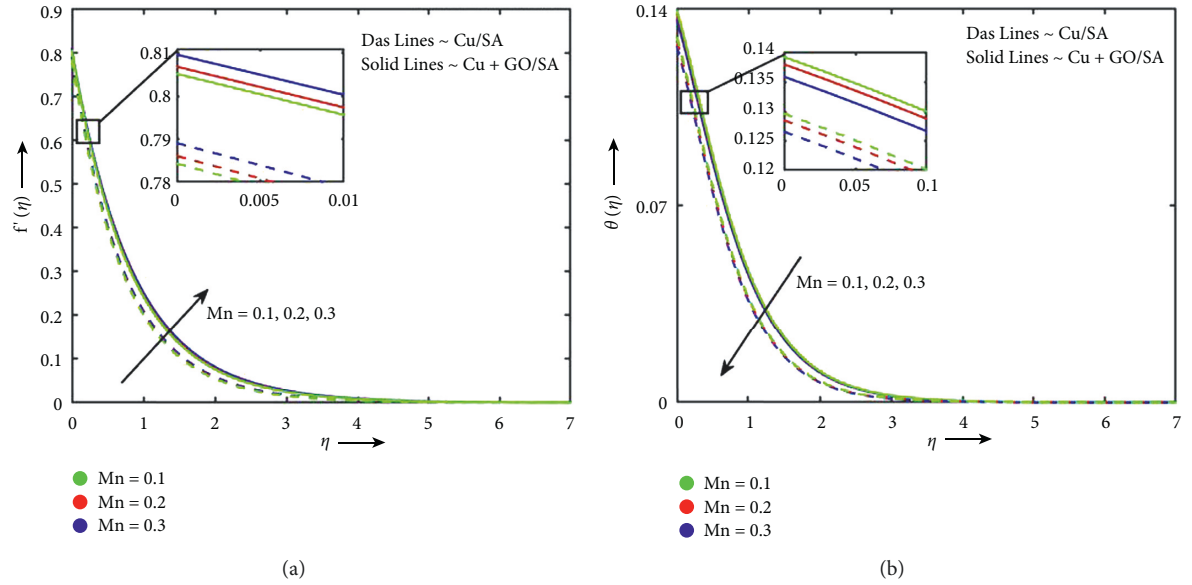

Figure 8: *Mn* variances in velocity and temperature.

consistencies. However, extremely accurate results for the current analysis are found.

4. Result and Discussion

Using the bvp4c technique, the characteristics of two different sodium alginate-based nanofluids, namely, $Cu - SA$ and $GO - Cu/SA$, are quantitatively examined. We compare our performance of the model to the analytical ones for the limited situation of standard Newtonian flow in the current configuration to validate our mathematical model. The effects of emerging flow characteristics are listed using various graphs and table data that have been compiled. The impact of multiple physical parameters on motion, temperature, skin-friction coefficient, and Nusselt parameter values obtained with MATLAB software is exposed in Figures 2–11 and Table 1. For the current research, we measured the values of physical parameters as $\beta = K = A = Nr = Ec = Q = Bi = 0.1$, $Mn = S = \Lambda = 0.2, \phi_{GO} = 0.09, \phi_{Cu} = 0.18$, and Pr $= 6.5$.

Figures 3(a) and 3(b) show the decline behavior of motion and temperature of increasing unsteadiness parameter, respectively, for both Cu/SA and $Cu - GO/SA$. Figure 3(b) shows how the unsteadiness affects the heat distribution, and it can be understood that as the unsteadiness number is raised, the temperature distribution drastically diminishes. This is true since a reduction in the temperature profile is brought on by an increase in heat

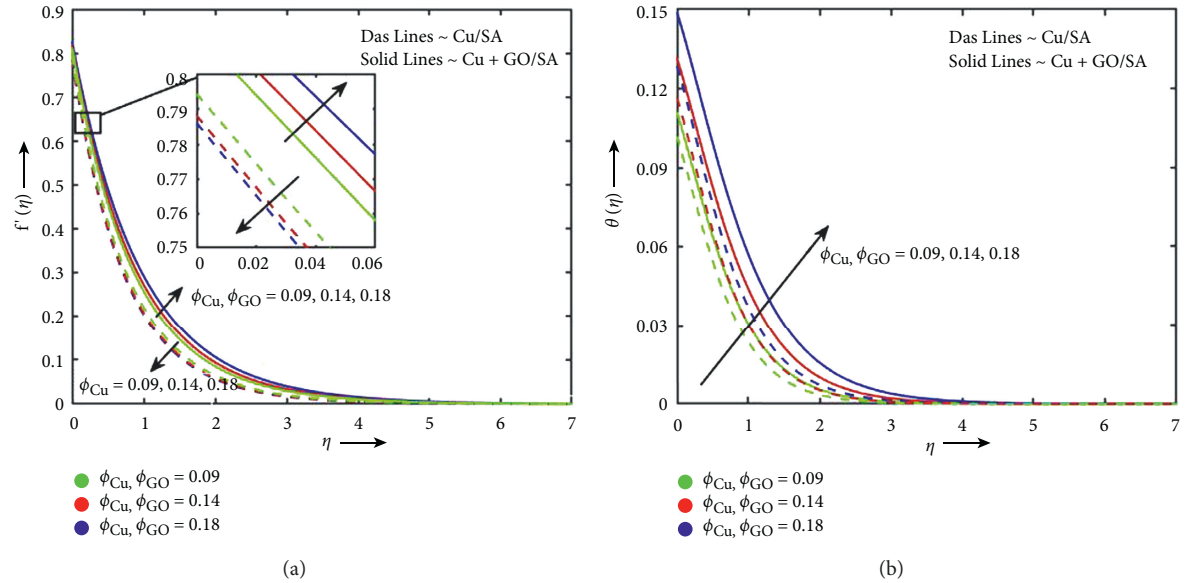

Figure 9: ϕ variances in velocity and temperature.

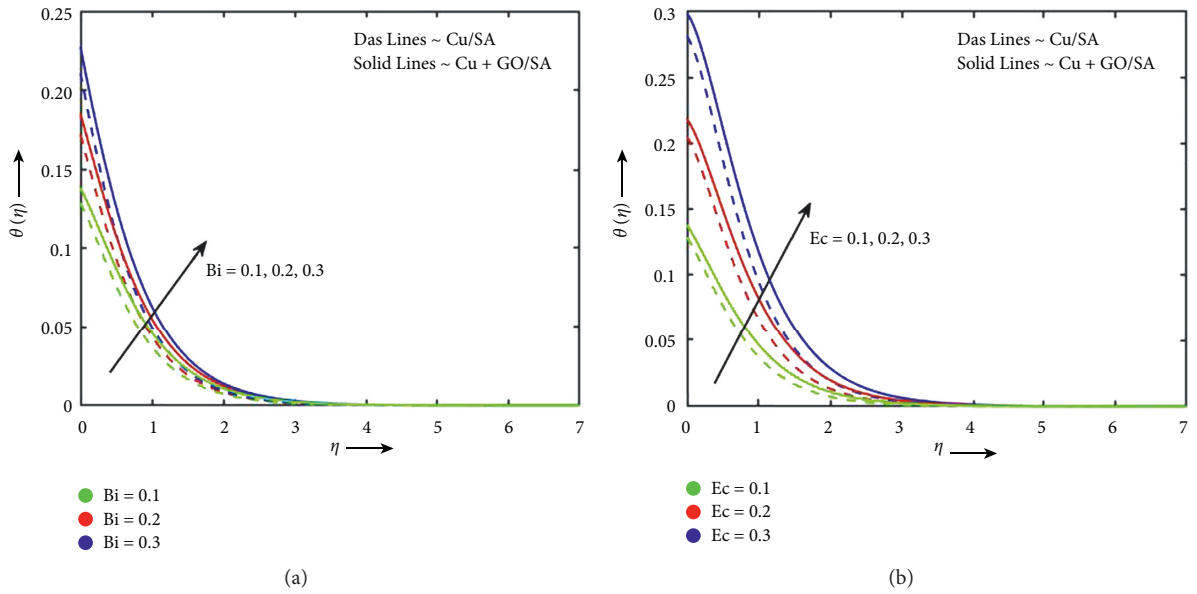

Figure 10: *Bi* and *Ec* variances in temperature.

losses of the sheet being stretched. Due to the reduction in the heat transference rate from the sheet to the fluid for larger quantities of the unsteady parameter, this suggests that the cooling rate is significantly greater than the rate of chilling for the steady flow.

Figures 4(a) and 4(b) depict the impression of the growing Deborah number on the velocity and temperature for both *Cu*/*SA* and *Cu* − *GO*/*SA*, respectively. Figure 4(a) shows how hybrid nanomaterials and nanostructures, as well as motion curves, are affected by the Deborah number. In comparison to the change in Deborah, the movement of nanoparticles and hybrid nanomaterials is decreased. This decrement flow behavior is caused by its elastic nature (Maxwell fluid). In light of fluid flow, Maxwell liquid repairs greater deformation as a result of this property. By using greater values of the Deborah number, momentum boundary layers are reduced. Additionally, it is looked at whether hybrid nanoparticles are more effective than approach-related nanomaterials in terms of maximum flow phenomena. Due to its elastic nature, flow properties are decreasing. Also, it is shown that Maxwell liquid is warmed up more than viscous fluid. In comparison to the instance of the technique associated with nanomaterials, it is noticed that the strategy associated with nanomaterials is much more effective in obtaining the greatest thermal energy (see Figure 4(b)).

In terms of flow behaviors, porosity has always played a key role. However, in nanolevel streaming settings, the

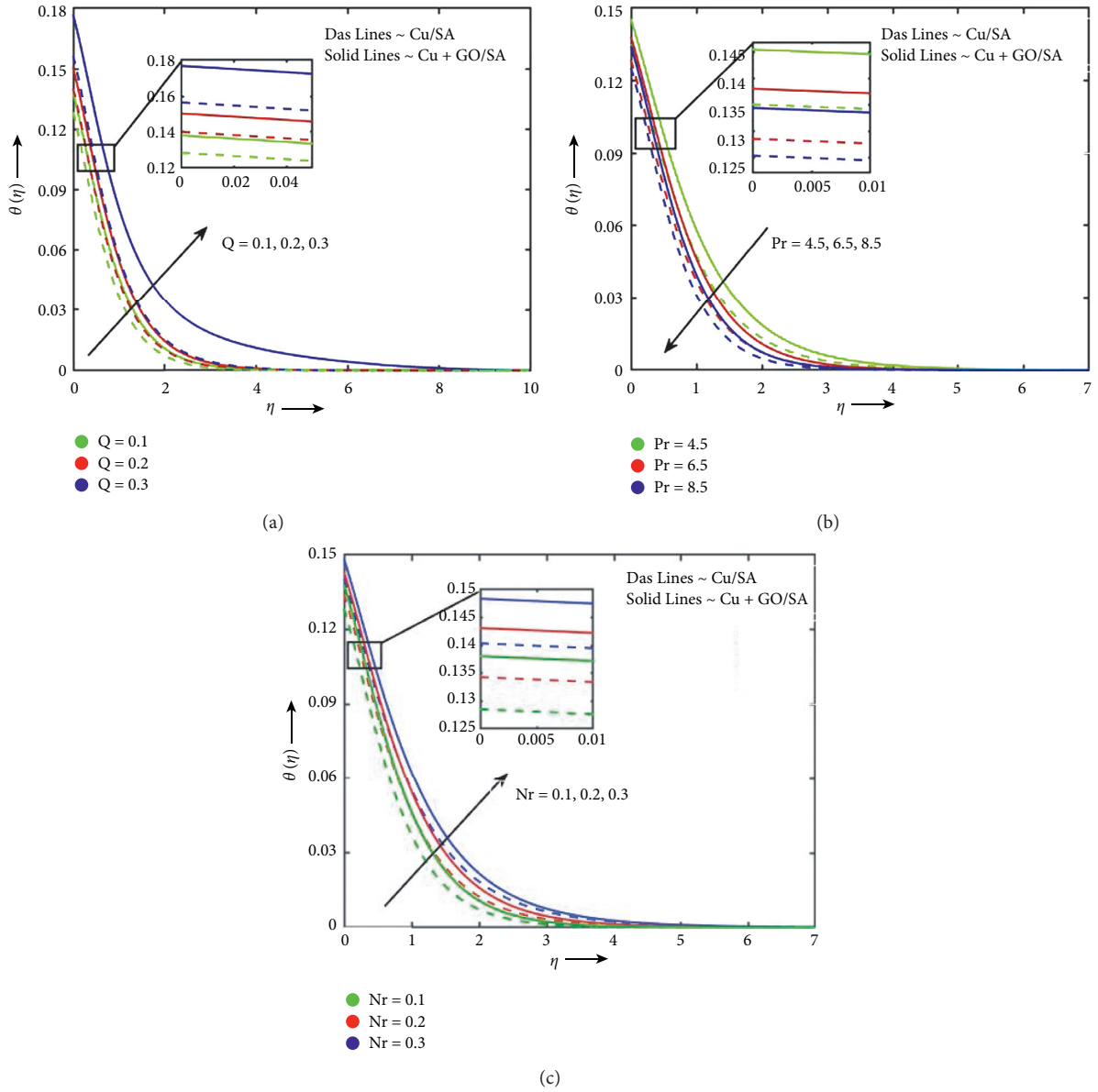

Figure 11: Q, Pr, and Nr variances in temperature.

porous nature of the material is critical for the passage of nanoparticles and thermal issues. $Cu - GO/SA$ hybrid nanofluid fluids continue to flow ahead of Cu/SA nanofluid fluids, as seen in Figure 5(a) when the porosity values increase. Fluids prefer to flow through the higher porosity rather than over it as the parameter continues to rise in value. In Figure 5(a), the flow rate for $hbnf$ is slower than that of nanolevel fluid because the flow seeks to flow into the porous mode more as there are more particles present. Both the $Cu - GO/SA$ mixture and the Cu/SA nanomixture of fluids are shown in Figure 5(b) in their most advanced thermal states. Two factors might be to blame for this increase: the first is the well-known explanation for lower fluidity absorbing more heat, the second is the special thermal transmitting properties of nanomaterials, and the $Cu - GO/SA$ hybrid is taking control of the Cu/SA by absorbing more heat, encouraging thermal dispersion of the hybrid. Because of the porous surface's ability to diminish fluidity, which lowers the fluid velocity and raises its heat, the porosity of the used fluid is directly related to its viscosity.

The impact of the suction ($+ve$ values) and injection ($-ve$ values) on the motion and temperature characteristics of both Cu/SA and Cu- GO/SA is depicted in Figure 6. As can be observed in Figure 6(a), as the suction impression is increased, the motion graphs and the thickness of the momentum boundary layer both decrease. However, when the injection parameter is increased, the velocity and momentum boundary layers are improved. Similar to this, as the suction variable is increased, the temperature profiles

Table 4: The skin-friction and Nusselt number values for Pr = 6.5.

β	Mn	K	A	Pr	Ec	Nr	Q	Bi	S	Λ	ϕ_{Cu}	ϕ_{GO}	$Cf_xRe_x^{1/2}$	$Nu_xRe_x^{-1/2}$
														0.203399471
														0.198911995
														0.193351315
														0.203103094
														0.203399471
														0.203900759
														0.203399471
														0.199526545
														0.195200657
													−2.007929558−2.218466432	0.203399471
													−2.462615810−2.025015280	0.206948785
													−2.007929558−1.978850427	0.210061001
													−2.007929558−2.224604383	0.201634394
													−2.449624474−2.007929558	0.203399471
													−2.186074026−2.386574079	0.204265376
													−2.007929543−2.007929558	0.203399471
													−2.007929560−2.007929558	0.184438877
0.1	0.2	0.1	0.1	6.5	0.1	0.1		0.1	0.2–0.4	0.2	0.18	0.09	−2.007929562−2.007929562	0.165478283
0.5	0.1	0.1	0.1	4.5	0.1	0.1	0.10.1	0.1	−0.2 0.2	0.1	0.09	0.09	−2.007929558−2.007929548	0.203399471
1	0.2	0.5	0.5	6.5	0.2	0.2	0.20.3	0.2	0.4	0.5	0.14	0.14	−2.007929543−2.007929558	0.220592104
	0.3	1	1	8.5	0.3	0.3		0.3		1	0.18	0.18	−2.007929554−2.007929541	0.237506074
													−2.007929558−2.007929556	0.203399471
													−2.007929554−1.512755614	0.200507438
													−1.658541706−2.007929558	0.194257513
													−2.215655645−2.304959505	0.203399471
													−1.470390874−1.036070950	0.384590061
													−1.504092052−1.924981668	0.547020898
													−2.330362054	0.197777437
														0.199618121
														0.203399471
														0.205201976
														0.199947269
														0.208729347
														0.211806558
														0.164188753
														0.21118982 9
														0.256863623

and the width of the thermal boundary layer decrease, but the reverse tendency is seen in the situation of blowing, as seen in Figure 6(b).

Fluid flow with $Cu - GO/SA$ and Cu/SA can have their flow rates restricted by the velocity slip constraint. The slip parameter slipperiness is overshadowed by the strength of solid materials, which is what would be causing the slow flow rate seen in Figure 7(a) for its boosted amounts. Figure 7(b) depicts the decline in temperature profiles of the upsurge velocity slip parameter.

As understood in Figure 8(a), the velocity rises as the magnetic field increases as a result of both Cu/SA and $Cu - GO/SA$ flow. Opposite impression is shown for temperature; that is, the temperature declines with growing magnetic (see Figure 8(b)).

Figure 9(a) depicts the influence of both Cu/SA and $Cu - GO/SA$ volumetric fraction parameters on velocity. The nanofluid flow slows down as the intensity increases. This occurrence occurs as a result of friction escalating, and fluid viscidness increases with increasing nanofluid volume fraction. As enhanced, the hybrid nanofluid has a faster motion than regular nanofluid. With increases in volume fraction, the fluid temperature rises noticeably, as seen in Figure 9(b). These conclusions support our concept that adding nanomaterials to regular fluids recovers thermal conductivity and increases thermal efficacy.

Figure 10(a) illustrates how the Biot quantity Bi raises the heat of the Maxwell graphene hybrid nanofluid and nanofluid. This may be explained by pointing out that an increase in Biot number grows in convective heat transport at the surface, which raises the temperature. It is evident from Figure 10(b) that raising Eckert quantities causes the heat flow to increase. The relationship Eckert establishes between enthalpy and kinetic energy and the reality that the

overall process is completed in the presence of viscidness while kinetic energy is converted to internal energy can both be used to clarify this characteristic of Maxwell fluid with copper and graphene nanospheres. As a result, viscous dissipation can raise a fluid temperature more quickly.

The thermal scatter in the $Cu - GO/SA$ and Cu/SA nanofluids is explained in Figure 11(a) to increase the heat generation constraint. According to the parameter, it tends to increase the flow's surrounding thermal conditions. This will demonstrate improved thermal diffusion for the two fluid flow combinations. The heat is seen to be decreasing in tendency while the Prandtl number is increasing in Figure 11(b). Failures in the heat curve are seen because the greater Prandtl number denotes the lower thermal diffusivity. The temperature of the $hbnf$ and nf grows better with an increase in radiation parameter, as shown in Figure 11(c). In reality, the radiation goes up the fluid ability to transfer heat, which causes the thermal boundary layer to expand and, as a consequence, lowers the fluid temperature.

Table 4 illustrates the various physical parameters values with skin-friction coefficient and heat transfer rate. The velocity declines and temperature increase when both nanoparticles have the same volume fraction value. The skin-friction coefficient declines with Deborah, unsteadiness, and porosity parameters, while the opposite behavior shows for the magnetic parameter. The Nusselt number upsurges with Prandtl, radiation, and Biot number. Both the thermal and motion impressions increase with the velocity slip parameter. The skin-friction declines, and temperature grows with suction/bowing influence.

5. Conclusions

The goal of the existing research is to boost the solar energy phenomenon, which will increase aircraft endurance and be employed in solar aviation for a variety of uses. Maxwell hybrid nanofluid is taken into consideration for this goal. Graphs and tables are thoroughly examined for many parametrical influences, including heat source, magnetic field, viscous dissipation, thermal liquid on PTSC, and solar-powered aircraft. The following are the findings that result from the issue mentioned:

(i) The upsurge in Deborah number reduces the skin-friction coefficient.

(ii) The heat source parameter declines the heat transfer rate but upsurges the skin-friction coefficient.

(iii) The skin-friction coefficient and heat transfer rate increase with growing magnetic impression.

(iv) The motion profile declines with Cu/SA and raises with $Cu - GO/SA$, while temperature grows for both hybrid nano- and nanofluids.

Data Availability

The raw data supporting the conclusions of this article will be made available by the corresponding author without undue reservation.

Conflicts of Interest

The authors declare that they have no conflicts of interest.

Authors' Contributions

All authors listed have made a substantial, direct, and intellectual contribution to the work and approved it for publication.

References

[1] M. Q. Brewster, *Thermal Radiative Transfer and Properties*, John Wiley & Sons, Hoboken, NJ, USA, 1992.

[2] S. U. Choi and J. A. Eastman, *Enhancing thermal Conductivity of Fluids with Nanoparticles (No. ANL/MSD/CP-84938; CONF-951135-29)*, Argonne National Lab. (ANL), Argonne, IL, USA, 1995.

[3] S. Suresh, K. P. Venkitaraj, P. Selvakumar, and M. Chandrasekar, "Effect of Al2O3–Cu/water hybrid nanofluid in heat transfer," *Experimental Thermal and Fluid Science*, vol. 38, pp. 54–60, 2012.

[4] X. Z. Gao, Z. X. Hou, Z. Guo, J. X. Liu, and X. Q. Chen, "Energy management strategy for solar-powered high-altitude long-endurance aircraft," *Energy Conversion and Management*, vol. 70, pp. 20–30, 2013.

[5] R. Barbosa, B. Escobar, V. M. Sanchez, J. Hernandez, R. Acosta, and Y. Verde, "Sizing of a solar/hydrogen system for high altitude long endurance aircrafts," *International Journal of Hydrogen Energy*, vol. 39, no. 29, Article ID 16637, 2014.

[6] J. Ahmad Khan, M. Mustafa, T. Hayat, and A. Alsaedi, "Numerical study of Cattaneo-Christov heat flux model for viscoelastic flow due to an exponentially stretching surface," *PLoS One*, vol. 10, no. 9, Article ID e0137363, 2015.

[7] S. Das, S. Chakraborty, R. N. Jana, and O. D. Makinde, "Entropy analysis of unsteady magneto-nanofluid flow past accelerating stretching sheet with convective boundary condition," *Applied Mathematics and Mechanics*, vol. 36, no. 12, pp. 1593–1610, 2015.

[8] J. Sarkar, P. Ghosh, and A. Adil, "A review on hybrid nanofluids: recent research, development and applications," *Renewable and Sustainable Energy Reviews*, vol. 43, pp. 164–177, 2015.

[9] D. Toghraie, V. A. Chaharsoghi, and M. Afrand, "Measurement of thermal conductivity of ZnO–TiO2/EG hybrid nanofluid," *Journal of Thermal Analysis and Calorimetry*, vol. 125, no. 1, pp. 527–535, 2016.

[10] U. Farooq, D. Lu, S. Munir, M. Ramzan, M. Suleman, and S. Hussain, "MHD flow of Maxwell fluid with nanomaterials due to an exponentially stretching surface," *Scientific Reports*, vol. 9, no. 1, pp. 7312–7411, 2019.

[11] K. Loganathan, S. Sivasankaran, M. Bhuvaneswari, and S. Rajan, "Second-order slip, cross-diffusion and chemical reaction effects on magneto-convection of Oldroyd-B liquid using Cattaneo–Christov heat flux with convective heating," *Journal of Thermal Analysis and Calorimetry*, vol. 136, no. 1, pp. 401–409, 2019.

[12] H. Maleki, J. Alsarraf, A. Moghanizadeh, H. Hajabdollahi, and M. R. Safaei, "Heat transfer and nanofluid flow over a porous plate with radiation and slip boundary conditions," *Journal of Central South University*, vol. 26, no. 5, pp. 1099–1115, 2019.

[13] Z. Abdelmalek, U. Nazir, M. Nawaz, J. Alebraheem, and A. Elmoasry, "Double diffusion in Carreau liquid suspended

with hybrid nanoparticles in the presence of heat generation and chemical reaction," *International Communications in Heat and Mass Transfer*, vol. 119, Article ID 104932, 2020.

[14] N. Khandelwal, M. Sharma, O. Singh, and A. K. Shukla, "Recent developments in integrated solar combined cycle power plants," *Journal of Thermal Science*, vol. 29, no. 2, pp. 298–322, 2020.

[15] K. Loganathan, K. M. Prabu, E. Elanchezhian, R. Nirmalkumar, and K. Manimekalai, "Computational analysis of thermally stratified mixed convective non-Newtonian fluid flow with radiation and chemical reaction impacts Journal of Physics: conference Series," *Journal of Physics: Conference Series*, vol. 1432, no. 1, Article ID 012048, 2020.

[16] F. Rubbi, K. Habib, R. Saidur, N. Aslfattahi, S. M. Yahya, and L. Das, "Performance optimization of a hybrid PV/T solar system using Soybean oil/MXene nanofluids as A new class of heat transfer fluids," *Solar Energy*, vol. 208, pp. 124–138, 2020.

[17] K. Loganathan, K. Mohana, M. Mohanraj, P. Sakthivel, and S. Rajan, "Impact of third-grade nanofluid flow across a convective surface in the presence of inclined Lorentz force: an approach to entropy optimization," *Journal of Thermal Analysis and Calorimetry*, vol. 144, no. 5, pp. 1935–1947, 2021.

[18] K. Loganathan, N. Alessa, K. Tamilvanan, and F. S. Alshammari, "Significances of Darcy–Forchheimer porous medium in third-grade nanofluid flow with entropy features," *The European Physical Journal - Special Topics*, vol. 230, no. 5, pp. 1293–1305, 2021.

[19] I. Waini, A. Ishak, T. Groşan, and I. Pop, "Mixed convection of a hybrid nanofluid flow along a vertical surface embedded in a porous medium," *International Communications in Heat and Mass Transfer*, vol. 114, Article ID 104565, 2020.

[20] M. Wu, Z. Shi, H. Ang, and T. Xiao, "Theoretical study on energy performance of a stratospheric solar aircraft with optimum Λ-shaped rotatable wing," *Aerospace Science and Technology*, vol. 98, Article ID 105670, 2020.

[21] F. Ahmad, S. Abdal, H. Ayed, S. Hussain, S. Salim, and A. O. Almatroud, "The improved thermal efficiency of Maxwell hybrid nanofluid comprising of graphene oxide plus silver/kerosene oil over stretching sheet," *Case Studies in Thermal Engineering*, vol. 27, Article ID 101257, 2021.

[22] S. Anitha, K. Loganathan, and M. Pichumani, "Approaches for modelling of industrial energy systems: correlation of heat transfer characteristics between magnetohydrodynamics hybrid nanofluids and performance analysis of industrial length-scale heat exchanger," *Journal of Thermal Analysis and Calorimetry*, vol. 144, no. 5, pp. 1783–1798, 2021.

[23] T. Gul, M. Bilal, M. Bilal, W. Alghamdi, M. I. Asjad, and T. Abdeljawad, "Hybrid nanofluid flow within the conical gap between the cone and the surface of a rotating disk," *Scientific Reports*, vol. 11, no. 1, pp. 1180–1219, 2021.

[24] A. Hussain, M. H. Alshbool, A. Abdussattar et al., "A computational model for hybrid nanofluid flow on a rotating surface in the existence of convective condition," *Case Studies in Thermal Engineering*, vol. 26, Article ID 101089, 2021.

[25] W. Jamshed, S. Uma Devi S, R. Safdar, F. Redouane, K. S. Nisar, and M. R. Eid, "Comprehensive analysis on copper-iron (II, III)/oxide-engine oil Casson nanofluid flowing and thermal features in parabolic trough solar collector," *Journal of Taibah University for Science*, vol. 15, no. 1, pp. 619–636, 2021.

[26] W. Jamshed, K. S. Nisar, R. W. Ibrahim, F. Shahzad, and M. R. Eid, "Thermal expansion optimization in solar aircraft using tangent hyperbolic hybrid nanofluid: a solar thermal application," *Journal of Materials Research and Technology*, vol. 14, pp. 985–1006, 2021.

[27] W. Jamshed, K. S. Nisar, S. S. P. M. Isa, S. Batool, A. H. Abdel-Aty, and M. Zakarya, "Computational case study on tangent hyperbolic hybrid nanofluid flow: single phase thermal investigation," *Case Studies in Thermal Engineering*, vol. 27, Article ID 101246, 2021.

[28] W. Jamshed, "Thermal Augmentation in Solar Aircraft Using tangent Hyperbolic Hybrid Nanofluid: A Solar Energy Application," *Energy & Environment*, 2021.

[29] K. Loganathan, G. Muhiuddin, A. M. Alanazi, F. S. Alshammari, B. M. Alqurashi, and S. Rajan, "Entropy optimization of third-grade nanofluid slip flow embedded in a porous sheet with zero mass flux and a non-Fourier heat flux model," *Frontiers in Physics*, vol. 8, p. 250, 2020.

[30] K. Loganathan, N. Alessa, N. Namgyel, and T. S. Karthik, "MHD flow of thermally radiative Maxwell fluid past a heated stretching sheet with Cattaneo–Christov dual diffusion," *Journal of Mathematics*, vol. 2021, Article ID 5562667, 10 pages, 2021.

[31] W. Jamshed, N. A. A. M. Nasir, S. S. P. M. Isa et al., "Thermal growth in solar water pump using Prandtl–Eyring hybrid nanofluid: a solar energy application," *Scientific Reports*, vol. 11, no. 1, Article ID 18704, 2021.

[32] K. Muhammad, T. Hayat, A. Alsaedi, and B. Ahmad, "Melting heat transfer in squeezing flow of basefluid (water), nanofluid (CNTs+ water) and hybrid nanofluid (CNTs+ CuO+ water)," *Journal of Thermal Analysis and Calorimetry*, vol. 143, no. 2, pp. 1157–1174, 2021.

[33] S. Qayyum, M. I. Khan, F. Masood, Y. M. Chu, S. Kadry, and M. Nazeer, "Interpretation of entropy generation in Williamson fluid flow with nonlinear thermal radiation and first-order velocity slip," *Mathematical Methods in the Applied Sciences*, vol. 44, no. 9, pp. 7756–7765, 2021.

[34] A. Saeed, M. Jawad, W. Alghamdi, S. Nasir, T. Gul, and P. Kumam, "Hybrid nanofluid flow through a spinning Darcy–Forchheimer porous space with thermal radiation," *Scientific Reports*, vol. 11, no. 1, pp. 16708–16715, 2021.

[35] N. A. Zainal, R. Nazar, K. Naganthran, and I. Pop, "Unsteady flow of a Maxwell hybrid nanofluid past a stretching/shrinking surface with thermal radiation effect," *Applied Mathematics and Mechanics*, vol. 42, no. 10, pp. 1511–1524, 2021.

[36] I. Ahmad, M. Faisal, Q. Zan-Ul-Abadin, T. Javed, and K. Loganathan, "Unsteady 3D heat transport in hybrid nanofluid containing brick shaped ceria and zinc-oxide nanocomposites with heat source/sink," *Nanocomposites*, vol. 8, no. 1, pp. 1–12, 2022.

[37] E. A. Algehyne, E. R. El-Zahar, S. H. Elhag et al., "Investigation of thermal performance of Maxwell hybrid nanofluid boundary value problem in vertical porous surface via finite element approach," *Scientific Reports*, vol. 12, no. 1, pp. 2335–2412, 2022.

[38] A. Bhattacharyya, R. Sharma, S. M. Hussain, A. J. Chamkha, and E. Mamatha, "A numerical and statistical approach to capture the flow characteristics of Maxwell hybrid nanofluid containing copper and graphene nanoparticles," *Chinese Journal of Physics*, vol. 77, pp. 1278–1290, 2022.

[39] S. Eswaramoorthi, K. Loganathan, R. Jain, and S. Gyeltshen, "Darcy-forchheimer 3D flow of glycerin-based carbon nanotubes on a Riga plate with nonlinear thermal radiation and cattaneo-christov heat flux," *Journal of Nanomaterials*, vol. 2022, Article ID 5286921, 20 pages, 2022.

[40] M. Ouni, L. M. Ladhar, M. Omri, W. Jamshed, and M. R. Eid, "Solar water-pump thermal analysis utilizing copper–gold/engine oil hybrid nanofluid flowing in parabolic trough solar collector: thermal case study," *Case Studies in Thermal Engineering*, vol. 30, Article ID 101756, 2022.

[41] F. Ali, K. Loganathan, S. Eswaramoorthi, K. Prabu, A. Zaib, and D. Kumar Chaudhary, "Heat transfer analysis on Carboxymethyl Cellulose water-based cross hybrid nanofluid flow with entropy generation & quot," *Journal of Nanomaterials*, vol. 2022, Article ID 5252918, 11 pages, 2022.

[42] I. Ahmad, Q. Zan-Ul-Abadin, M. Faisal, K. Loganathan, T. Javed, and D. Kumar Chaudhary, "Quot; prescribed thermal activity in the radiative bidirectional flow of magnetized hybrid nanofluid: keller-box Approach & quot," *Journal of Nanomaterials*, vol. 2022, Article ID 5531041, 16 pages, 2022.

[43] I. Ahmad, Q. Zan-Ul-Abadin, M. Faisal, K. Loganathan, T. Javed, and N. Namgyel, "Convective heat transport in bidirectional water driven hybrid nanofluid using blade shaped Cadmium Telluride and graphite nanoparticles under electromagnetohydrodynamics process," *Journal of Mathematics*, vol. 2022, Article ID 4471450, 14 pages, 2022.

[44] I. Ahmad, Q. Zan-Ul-Abadin, M. Faisal, K. Loganathan, T. Javed, and S. Gyeltshen, "Entropy analysis in bidirectional hybrid nanofluid containing nanospheres with variable thermal activity," *Journal of Nanomaterials*, vol. 2022, Article ID 1915185, 15 pages, 2022.

[45] S. M. Hussain, "Dynamics of radiative Williamson hybrid nanofluid with entropy generation: significance in solar aircraft," *Scientific Reports*, vol. 12, no. 1, pp. 8916–8923, 2022.

[46] W. Jamshed, S. U. DeviS, M. Prakash et al., "Entropy amplified solitary phase relative probe on engine oil-based hybrid nanofluid," *Chinese Journal of Physics*, vol. 77, pp. 1654–1681, 2022.